COSMIC RANDOM WALKS UNDERLYING AN INFINITE-GENUS UNIVERSE

Arturo Tozzi
Center for Nonlinear Science, University of North Texas
1155 Union Circle, #311427
Denton, TX 76203-5017, USA, and
Computational Intelligence Laboratory, University of Manitoba, Winnipeg, Canada
Winnipeg R3T 5V6 Manitoba
tozziarturo@libero.it
Arturo.Tozzi@unt.edu

Alexander Yurkin
Russian Academy of Sciences
Moscow, Puschino, Russia
alvl1yurkin@rambler.ru

James F. Peters
Department of Electrical and Computer Engineering, University of Manitoba
75A Chancellor's Circle, Winnipeg, MB R3T 5V6, Canada and
Department of Mathematics, Adıyaman University, 02040 Adıyaman, Turkey,
Department of Mathematics, Faculty of Arts and Sciences, Adıyaman University
02040 Adıyaman, Turkey and Computational Intelligence Laboratory, University of
Manitoba, WPG, MB, R3T 5V6, Canada
james.peters3@umanitoba.ca

The Universe, rather than being homogeneous, displays an almost infinite topological genus, because it is punctured with a countless number of gravitational vortexes, i.e., black holes. Starting from this view, we aim to show that the occurrence of black holes is constrained by geometric random walks taking place during cosmic inflationary expansion. At first, we introduce a visual model, based on the Pascal's triangle and linear and nonlinear arithmetic octahedrons, which describes three-dimensional cosmic random walks. In case of nonlinear 3D paths, trajectories in an expanding Universe can be depicted as the operation of filling the numbers of the octahedrons in the form of "islands of numbers": this leads to separate cosmic structures (standing for matter/energy), spaced out by empty areas (constituted by black holes and dark matter). These procedures allow us to describe the topology of an universe of infinite genus, to assess black hole formation in terms of infinite Betti numbers, to highlight how non-linear random walks might provoke gravitational effects also in absence of mass/energy, and to propose a novel interpretation of Beckenstein-Hawking entropy: it is proportional to the surface, rather than the volume, of a black hole, because the latter does not contain information.

Keywords: arithmetic figures, black hole, deterministic model, geometrization of physics, random walk.

In this paper, we will tackle the issue of a scarcely observed cosmic topological property. The most successful accounts, including Einstein's (1905), implicitly assume that the Universe is a Riemannian manifold with genus zero. Genus is a particular topological invariant, generally used for classification of 2D manifolds, linked to the Euler characteristic, which generalizes to higher dimensions. However, the Universe displays countless holes, *i.e.*, the spacetime punctures of its own structure called black holes. This means that the Universe is equipped a countless, or at least very high, number of holes, and, assuming that it is isotropic and homogeneous at very large scales, the cosmic displacement of black holes might be regular. To make a trivial example, we might think to the spacetime fabric as a sponge equipped with countless, uniformly placed, holes.

Therefore, we ask: what are, and how are cosmic vortexes produced, within the geometric dynamics on a 3D manifold of infinite genus? What are the topological features, peculiarities and predictable physical consequences of a Universe described in terms of a Riemannian manifold with very high, almost infinite, genus? To answer these questions, we introduce a deterministic geometric model that permits visual constructions of linear (without any acceleration) and nonlinear (with the simplest uniformly acceleration) random walks in three-dimensional spaces. Our model is derived from the Pascal's triangle, an array of the binomial coefficients widely used in numerous contexts. Its applications in mathematics extend to algebra, calculus, trigonometry, plane and solid geometry. Two major areas where Pascal's Triangle is used, are algebra and probability/combinatorics (Edwards 2013). It is a useful tool in finding, without tedious computations, the number of subsets of r elements that can be formed from a set with n distinct elements (Brothers 2012). In the real world, this leads into the complex topic of graph theory (turning mapping information into structures such as

shortest paths, Dijkstra's algorithm, airplane routes and airport control, computer graphics, engineering, data management and search algorithms). In a triangular portion of a grid, the number of shortest grid paths from a given node to the top node of the triangle is the corresponding entry in Pascal's triangle. The pattern produced by an elementary cellular automaton using rule 60 is exactly the Pascal's triangle of binomial coefficients reduced modulo 2. Further, to provide a last example, Proton Nuclear Magnetic Resonance displays an inherent geometry in which Pascal's triangles have a prominent role (Hore 1983).
In the following, we will show how Pascal's triangle-derived models are able to describe the paths of random walks in an expanding universe and to explain the formation of black holes. Also, we calculate pure mathematics models without gravitation, considering that non-linear random walks may stand for motion with acceleration able to give rise to the the effect of cosmic gravity.

GEOMETRIC MODEL OF RANDOM WALKS

Simple and visual geometric models are needed to to substantiate the consistency in describing complex phenomena (Klein 1956; Sommerfeld 1973). Here we propose various recursive formulas for calculating the step-shaped Pascal's triangle at various initial conditions, to assess cosmic random walks processes.
Pascal's arithmetic triangle, its analogues, generalizations and possible applications of visual geometric models have been thoroughly carried out (Yurkin, 2013, 2016, 2018; Yurkin et al., 2018). Novel, stepwise form for Pascal's triangle (1D), two-sided (2D) and multidimensional generalizations can be achieved, both in linear and nonlinear random walks' models (Kolmogorov et al., 1995). Yurkin (1995) proposed an optical laser scheme that is a nonlinear 1D walk in a system of rays; further, a real laser nonlinear 2D random walk in a system of rays was carried out. Nonlinear and non-Markovian random walks were described by Fedotov and Korabel (2015). Sarkar an Maiti (2017) described a symmetric random walk on a regular tetrahedron, an octahedron and a cube. In the 1D case (along a straight line) (Kolmogorov et al., 1995), a random walk (linear and nonlinear) can occur along two mutually perpendicular directions (right, left) inside an arithmetic triangle (the triangle has two corners on his base and one on his top). In the 2D case (Yurkin 2019), a random walk (linear and nonlinear) can be carried out in four different directions (forward, back, right, left) inside an arithmetic square (the square has four corners).
In this paper, we aim to assess visual linear and nonlinear 3D models in form of arithmetic octahedrons to describe linear and nonlinear 3D random walks. In the 3D case of a Pascal's triangle, a random walk (linear and nonlinear) can be carried out in six different directions (forward, backward, right, left, up, down) inside an octahedron equipped with six vertices.

Linear random 3D walk in the octahedron. A 3D linear random walk or a walk in a volume can be described using a 3D model in the form of an arithmetic regular octahedron. We achieve the linear binomial coefficients in the computed cell of the octahedron n by summing the numbers from the six cells adjacent to the computed cell.
Figures 1-4 show sequentially, for the first four iterations, images of linear arithmetic octahedrons composed of small cubes. The parts of the **Figures 1-4** termed with (a) show images of the arithmetic octahedrons themselves, while (b) show images of layers of octahedrons composed of small cubes containing numbers. These numbers correspond to the number of walks from the initial cell (initial cube) to the final cell (final cube).

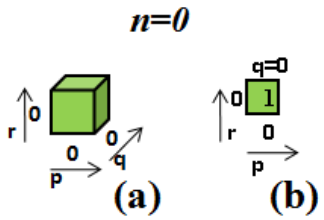

Figure 1. The zero linear arithmetic octahedron (zero iteration $n = 0$) consists of 1 cube.

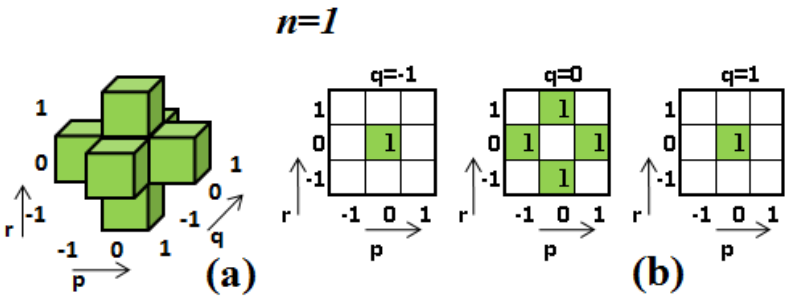

Figure 2. The first linear arithmetic octahedron (the first iteration $n = 1$) consists of 6 cubes.

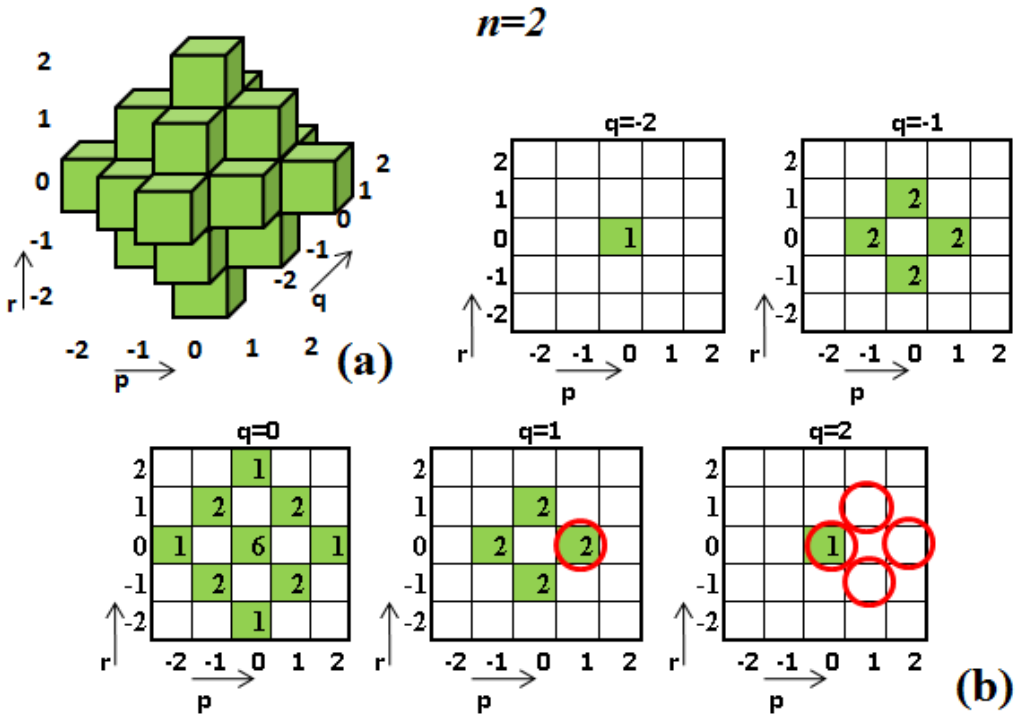

Figure 3. The second linear arithmetic octahedron (second iteration $n = 2$) consists of 19 cubes.

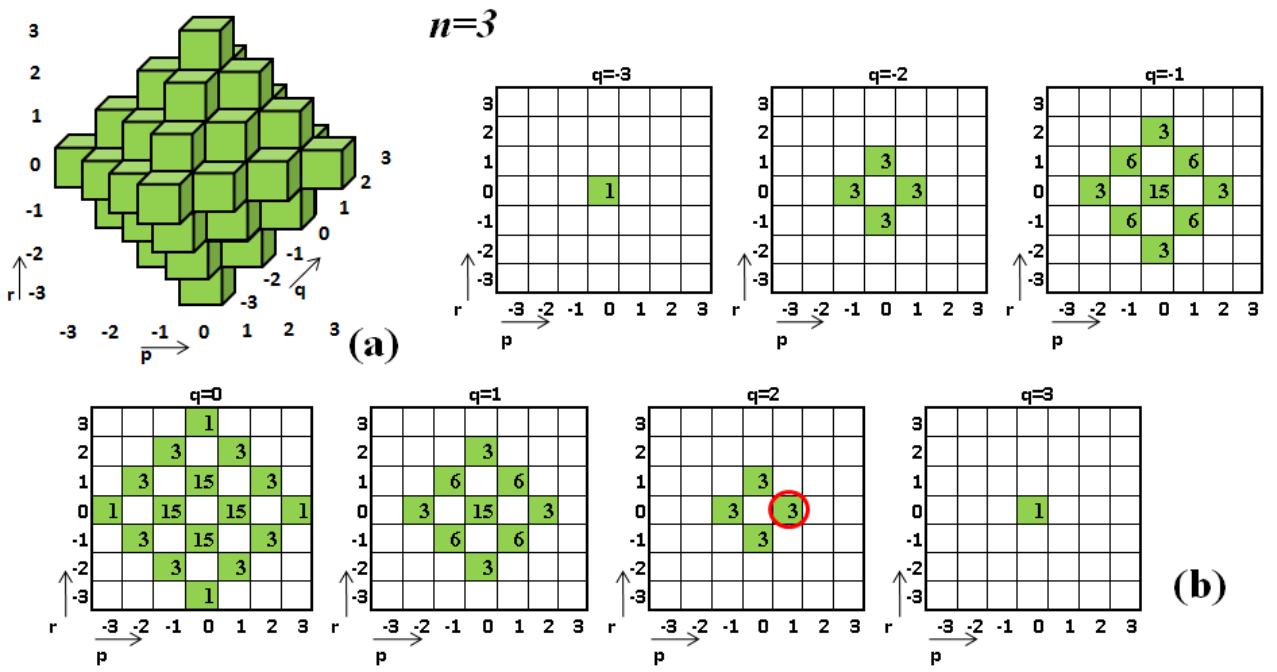

Figure 4. The third linear arithmetic octahedron (the third iteration $n = 3$) consists of 44 cubes.

The sequence of numbers of octahedrons in the example is denoted by$n: = 0, 1, 2, \ldots$. The total sum of numbers in octahedrons is 6^n. The numbers characterizing the octahedron (which describe the location of the cubes composing the octahedron) are denoted p, q and r:

$$p = 0, \pm1, \pm2, \ldots, \pm n; q = 0, \pm1, \pm2, \ldots, \pm n: r = 0, \pm1, \pm2, \ldots, \pm n. \quad (1)$$

Denote a number located in the n – octahedron as $\binom{n}{p}{q}{r}$, then specify the number of the zero octahedron($n = 0$), or, in other words, the initial conditions:

$$\binom{0}{p}{q}{r} = 1 \text{for } p = 0, q = 0, r = 0 \text{ and } \binom{0}{p}{q}{r} = 0 \quad (2)$$

for the other values p, q and r.

The numbers in the linear arithmetic octahedron are linear binomial coefficients $\binom{n}{p}{q}{r}$. They can be can be calculatedusing the recursive 3D linear expression:

$$\binom{n}{p}{q}{r} = \binom{n-1}{p}{q-1}{r} + \binom{n-1}{p}{q}{r+1} + \binom{n-1}{p-1}{q}{r} + \binom{n-1}{p+1}{q}{r} + \binom{n-1}{p}{q}{r-1} + \binom{n-1}{p}{q+1}{r}. \quad (3)$$

Example 1: $n = 3, p = 1, q = 2, r = 0$.

$$\binom{3}{1}{2}{0} = \binom{2}{1}{1}{0} + \binom{2}{1}{2}{1} + \binom{2}{0}{2}{0} + \binom{2}{2}{2}{0} + \binom{2}{1}{2}{-1} + \binom{2}{1}{3}{0} = 3,$$

as

$$\binom{2}{1}{1}{0} = 2, \binom{2}{1}{2}{1} = 0, \binom{2}{0}{2}{0} = 1, \binom{2}{2}{2}{0} = 0, \binom{2}{1}{2}{-1} = 0, \binom{2}{1}{3}{0} = 0.$$

In **Figures 3** and **4**, these numbers are circled in red circle, except for the number $\binom{2}{1}_{3}^{0} = 0$, which goes beyond the square in **Figure 3** in accordance with the expression (13); for this number: $q = 3 > n = 2$.

Figures 2-4 show that the octahedrons are densely filled with green cubes (branching cells). Neighboring empty cells inside octahedrons (white cubes or gaps) will be filled with green cubes at the next iteration. We can say that numbers densely (without spaces) fill the linear arithmetic octahedrons).

Nonlinear random 3D walk in the octahedron. To describe a nonlinear 3D random walk, we calculate nonlinear coefficients using the recursion formula given below and check it in the Figures. A 3D nonlinear random walk or a walk in a volume can also be described, like a linear one, using a 3D model in the form of a nonlinear arithmetic regular octahedron. Nonlinear binomial coefficients in the computed cell of the octahedron $n = 1$ are obtained by summing the numbers of six cells adjacent to the computed cell; nonlinear binomial coefficients in the cell of the octahedron $n = 2$ we get by summing the numbers of six cells located one through the calculated cell; nonlinear binomial coefficients in the cell of the octahedron $n = 3$ we get by summing the numbers of six cells located two through the calculated cell; etc.
Figures 5-8 show sequentially (for the first four iterations) images of the nonlinear arithmetic octahedrons composed of small cubes. **Figures 5-8** termed with (a) show images of the arithmetic octahedrons themselves, while (b) show images of layers of octahedrons composed of cubes containing numbers. These numbers correspond to the number of walks from the initial cell (initial cube) to the final cell (final cube).

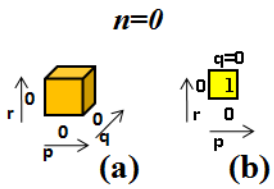

Figure 5. The zero nonlinear arithmetic octahedron (zero iteration $n = 0$) consists of 1 cube.

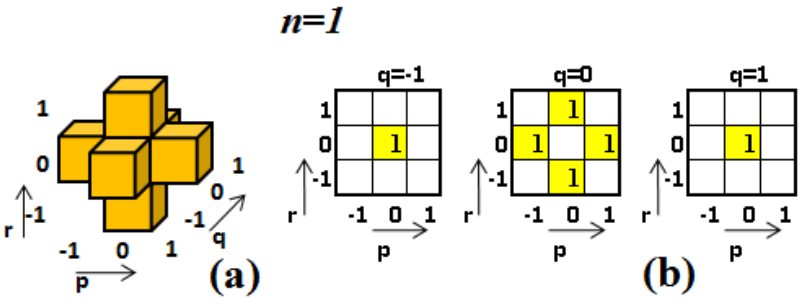

Figure 6. The first nonlinear arithmetic octahedron (the first iteration $n = 1$) consists of 6 cubes.

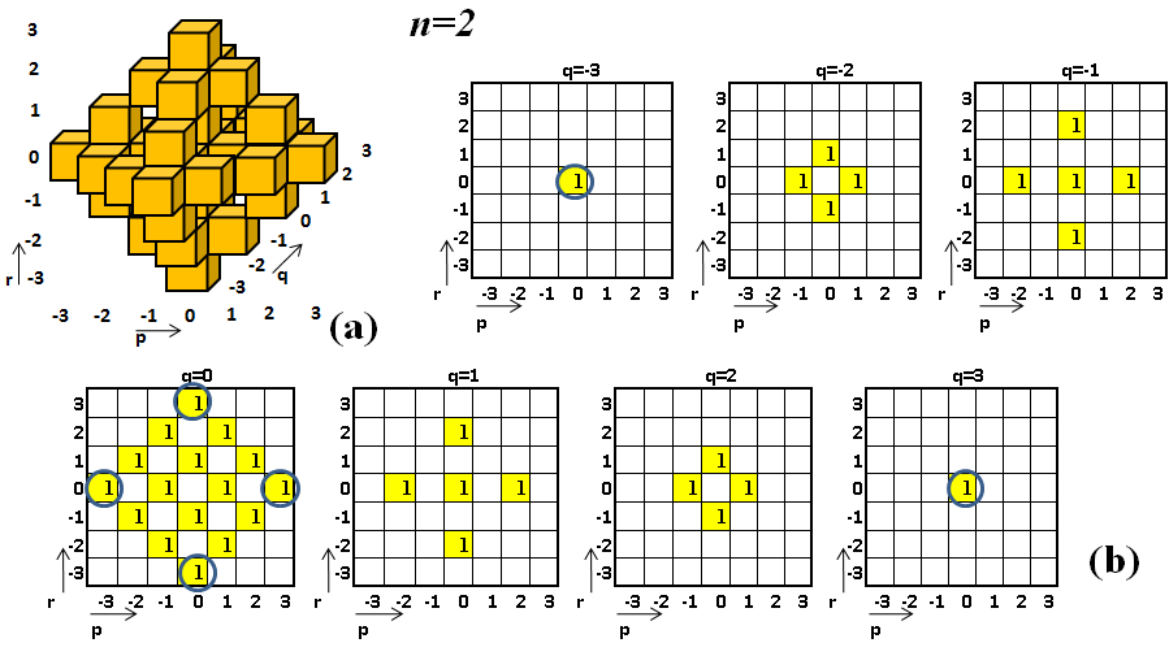

Figure 7. The second nonlinear arithmetic octahedron (the second iteration $n = 2$) consists of 36 cubes. The Figures $q = \pm 1$ clearly show the formation of separate structures of numbers ("islands of numbers").

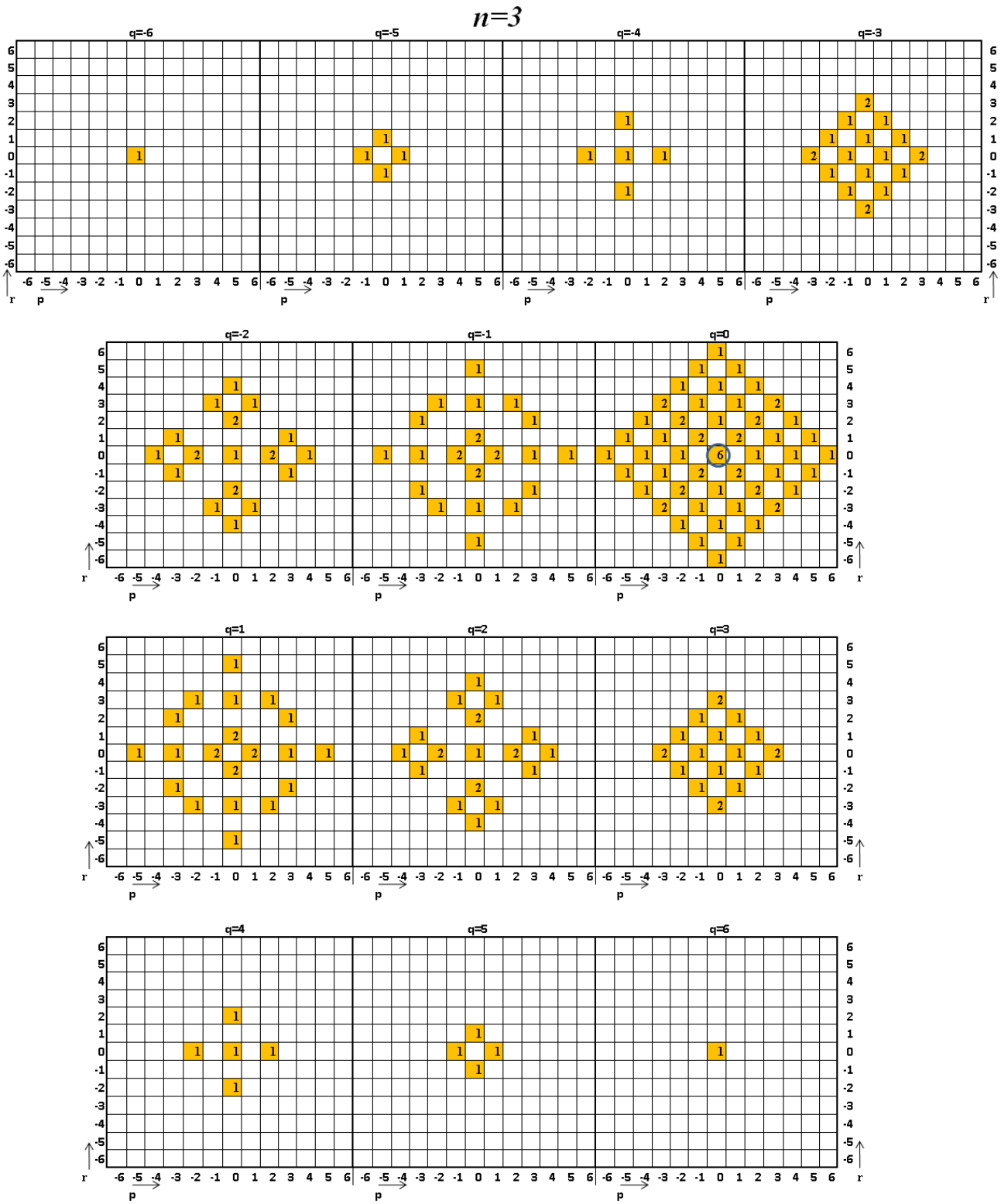

Figure 8. The third nonlinear arithmetic octahedron (the third iteration $n = 3$) consists of 175 cubes. The Figures $q = \pm 1, q = \pm 2, q = \pm 4$ clearly show the formation of separate structures of numbers ("islands of numbers"). The image of the corresponding octahedron is not dispalyed.

The sequence of numbers of octahedrons (rows of numbers in the octahedron) for the 3D case in this example is denoted by n: $n = 0, 1, 2, \ldots$. The total sum of numbers in octahedron is 6^n. The numbers characterizing the nonlinear octahedron (the numbers illustrating the position of the cubes of which the octahedron is composed) are denoted by p, q and r:

$$\left.\begin{array}{c} p = 0, \pm 1, \pm 2, \ldots, \pm n(n+1)/2; \\ q = 0, \pm 1, \pm 2, \ldots, \pm n(n+1)/2; \\ r = 0, \pm 1, \pm 2, \ldots, \pm n(n+1)/2. \end{array}\right\} \quad (4)$$

Denote a number located in the n - octahedron as $\binom{n}{p}_{q}^{r}$ then specifies the number of the zero octahedron ($n = 0$), or in other words, the initial conditions:

$$\binom{0}{p}_{q}^{r} = 1 \text{for } p = 0, q = 0, r = 0 \text{ and } \binom{0}{p}_{q}^{r} = 0 \quad (5)$$

for the other values of p, q and r.

The numbers in the nonlinear arithmetic octahedron are nonlinear binomial coefficients $\binom{n}{p}_{q}^{r}$, *which* can be found using the recursive 3D nonlinear expression:

$$\binom{n}{p}_{q}^{r} = \binom{n-1}{p}_{q-n}^{r} + \binom{n-1}{p}_{q}^{r+n} + \binom{n-1}{p-n}_{q}^{r} + \binom{n-1}{p+n}_{q}^{r} + \binom{n-1}{p}_{q}^{r-n} + \binom{n-1}{p}_{q+n}^{r}. \quad (6)$$

Example 2: $n = 3, p = 0, q = 0, r = 0$.

$$\binom{3}{0}_{0}^{0} = \binom{2}{0}_{-3}^{0} + \binom{2}{0}_{0}^{3} + \binom{2}{-3}_{0}^{0} + \binom{2}{3}_{0}^{0} + \binom{2}{0}_{0}^{-3} + \binom{2}{0}_{3}^{0} = 6,$$

as

$$\binom{2}{0}_{-3}^{0} = 1, \binom{2}{0}_{0}^{3} = 1, \binom{2}{-3}_{0}^{0} = 1, \binom{2}{3}_{0}^{0} = 1, \binom{2}{0}_{0}^{-3} = 1, \binom{2}{0}_{3}^{0} = 1.$$

In **Figures 7-8**, these numbers are circled in blue.

Figures 6-8 illustrate that the octahedrons are not tightly filled with yellow cubes (branching cells). Some empty cells inside the octahedrons (white cubes or gaps) will be filled with yellow cubes at the next iteration, and some empty cells will be filled after several iterations, and some empty cells will be filled after many iterations, and so on. Our numerical calculations show that for big n numbers the relative quantity of the empty cells or gaps (relative to the general quantity of cells in nonlinear octahedron) decreases with n increasing.

COSMIC RANDOM WALKS

The results achieved in the previous paragraphs allow the classification of different types of random walks in the form of the following table:

	Linear random walk (one unit steps, perpendicular each others)	**Nonlinear random walk** (first one unit steps, second two units steps, third three unit steps, ets., perpendicular each others)
3D case	• Steps of constant length along six perpendicular directions in octahedron. • Gaps and "islands of numbers" are absent in a linear arithmetic octahedron.	• Steps of increasing length along six perpendicular directions in octahedron. • Gaps and "islands of numbers" appear and disappear in different areas in a nonlinear arithmetic octahedron after several or many iterations. The relative quantity of the empty cells or gaps decreases with n increasing.

The above-described Pascal's triangle-framed geometric linear and nonlinear constructions and recursive formulas may find application to understand the development of black holes and dark matter in an expanding universe, starting from 3D random walks. The filled cells stand for matter/energy progressively expanding in an inflated universe, while the empty cells progressively produced inside the octahedrons stand for newly-generated black holes and dark matter, which number progressively increases (**Figure 9**). At the next iterations, the empty cells will be progressively filled with yellow cubes: this means that black holes continuosly appear and disappear, when further iterations take place during the expansion of the Universe.

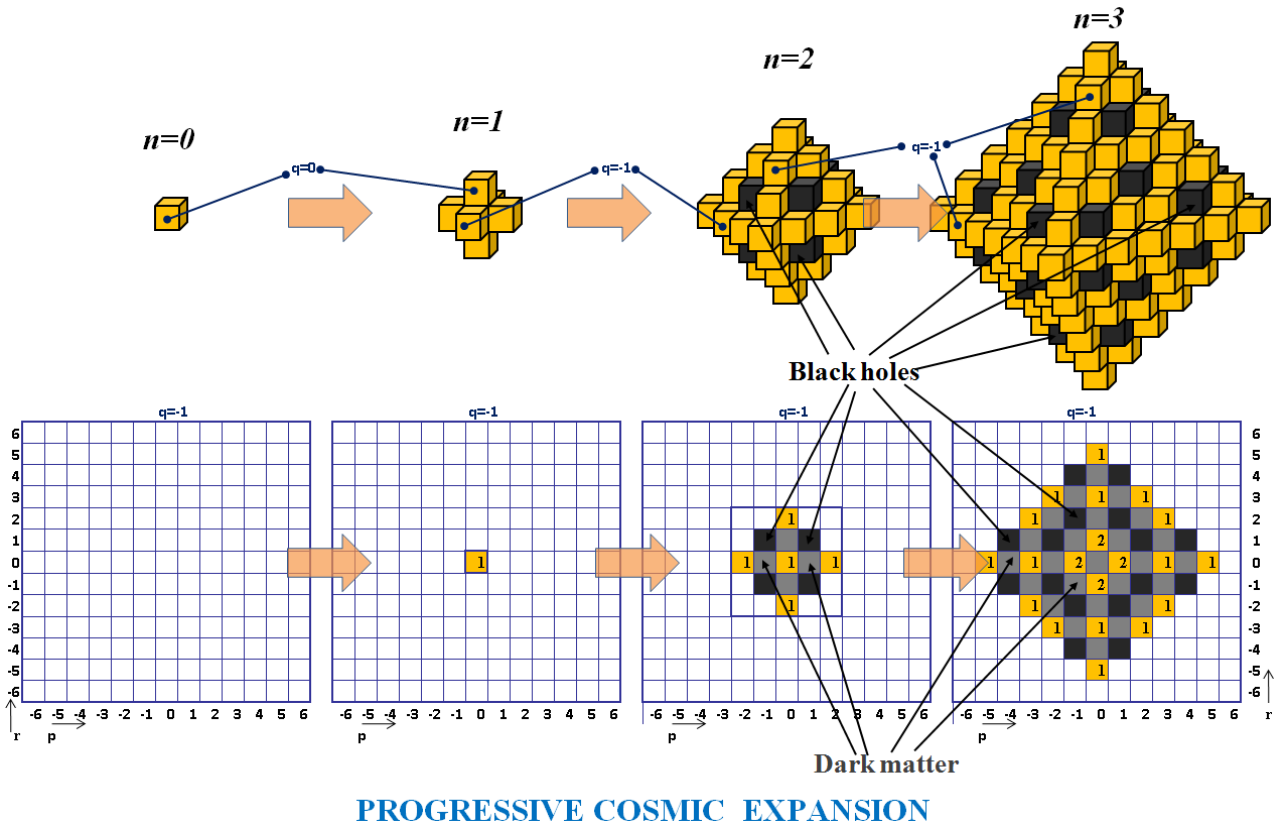

Figure 9. Cosmic expansion and black holes/dark matter formation in terms of random walks taking place inside a 3D lattice. It is noteworthy that dark matter can also contain its black holes, which in our octahedron model look like gaps too.

Vortex cycles. A punctured manifold is analogous to a cosmic physical space with holes. This means that we need to work on a manifold that is Riemannian. Briefly, a manifold is a topological space that is locally Euclidean (i.e., around

every point, there is a neighborhood that is topologically the same as the open unit ball in R^n). A Riemann surface is a surface-like configuration that covers the complex plane with several, and in general infinitely many, "sheets". A sample Riemannian surface is shown in **Figure 10**. It is easy to notice that the center of the surface is punctured with a hole, which stands, in our framework, for a spacetime rupture due to a black hole.
With a black hole, we need to consider gravitational pull, which is quite a bit more than a Riemann surface offers. A black hole can be modelled as a vortex cycle (Peters, 2018; Peters, 2019) with induced order proximity of spiraling hole vortexes (Ahmad and Peters, 2019). The rim of a cosmic vortex cycle represents the edge of a black hole. The inner cycles for a vortex reaching inward represent gravitational pull. Therefore, cosmos can be depited as nesting, non-concentric vortex cycles embedded in a punctured Riemann surface (Weyl, 1955).

In this context, a novel formulation of the Borsuk Ulam theorem might be of great help: the Vortex-BUT, which works on a manifold with holes. There are three forms of vortexBUT:

- physical geometry vortex BUT (pevBUT): each pair of antipodal vortex surface points map to R^n.
- region-based vortex BUT (revBUT): each pair of antipodal vortex region points map to R^n.
- descriptive vortex BUT (phivBUT): each pair of anitipodal vortex surface points OR regions maps to R^k, k >= 1.

Each black hole is an example of a massive vortex cycle. A punctured physical surface is a surface populated by vortices: this allows us to start viewing punctured cosmos surfaces using vortexBUT. The one very different thing about the new form of BUT is that we replace the Borsuk-Ulam use of S^n with V^n, a vortex in n-dimensional space. Then the simplest form of vortexBUT is defined by a continuous function

f: $V^n \rightarrow R^n$

so that f(x) = f(-x) for antipodal points x,-x on V^n.

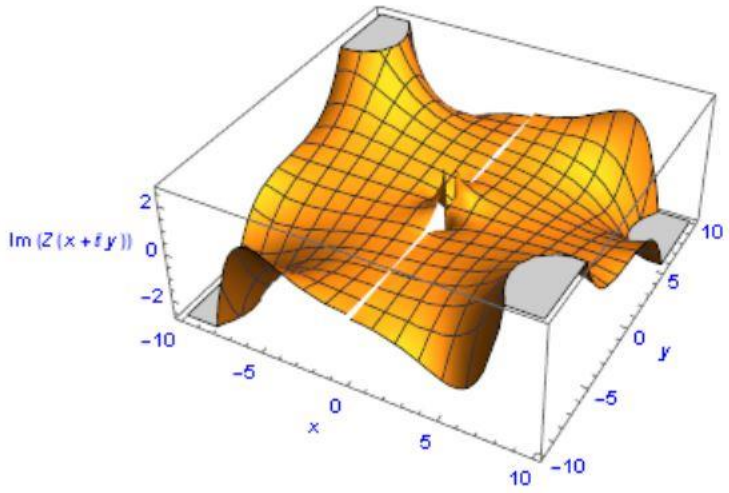

Figure 10. A Riemannian surface with the center of the surface punctured with a hole.

CONCLUSIONS

Our studies of deterministic models and visual constructions of linear (without any acceleration) and nonlinear (with the simplest uniformly acceleration) 3D random walks through arithmetic figures show various interesting geometric properties. In 3D spaces encompassing linear random walks, the achieved arithmetic octahedron is densely filled with numbers (**Figures 2 – 4**). In 3D spaces encompassing nonlinear random walks, the achieved arithmetic octahedron is not completely filled with numbers, i.e., it contains gaps. Indeed, some neighboring regions inside the nonlinear octahedron remain empty until either the very next iteration, or during several or many iterations. Gaps and "islands of numbers" or separate structures of numbers consistently appear and disappear after several or many iterations in the nonlinear 3D case (**Figures 6–8**). For high n numbers, the relative quantity of the empty cells or gaps (relative to the general quantity of cells in nonlinear octahedron) decreases with n increasing. In sum, for nonlinear 3D cases, we can speak of filling the numbers of the arithmetic octahedron in the form of "islands of numbers" or separate structures of numbers: this leads us into the realm of an homogeneous universe punctured with black holes that break the topological structure of the spacetime. In our framework, the combinatorial properties of the Pascal's triangle are the mathermatical operations that lead to cosmic expansion, through iterated random walk patterns. The occurrence of black holes in terms of "hollows" in the very structure of the spacetime allows us to consider the topological features of a high-genus manifold, compared with genus-zero manifolds. What does the occurrence of a cosmic manifold of very high genus physically mean? The Universe is a dynamical system where the genus changes continuously, because black holes are created or evaporate. If the Universe displays high genus, the big crunch cannot occur, because the squeezing of the spacetime leaves always holes, that cannot be reduced to a single point. The occurrence of high genus might help to draw other theoretical previsions. Our numerical calculations show that, for big n numbers, the relative quantity of the empty cells or gaps (relative to the general quantity of cells in nonlinear octahedron) decreases with n increasing. This means that the number of black holes, in cosmic timescales, will tend to decrease.

The canonical account of black holes's formation describes contracting stars, which give rise to mass accretion able to bend spacetime, until a black hole is produced. Our model provides another way to generate black holes: the progressive iterations of random walks in an expanding universe lead to the production of hollows, standing for places where an estreme spacetime curvature occurs as first event. Reversing the standard account, the curvature deformation attracts matter, and not viceversa. Therefore, according to our account, black hole formation migth occur in absence of gravitational effects provoked by mass/energy concentration which deform spacetime's curvatures. Indeed, the same gravitational effects can be gained through another mechanism, i.e., movements equipped with acceleration. To make an example, pilots performing maneuvers receive very strong overloads: 5 – 10 g, where g is acceleration of gravity to Earth. But pilots receive overloads 5 – 10 times higher than Earth attraction not because Earth suddenly began to attract them stronger, rather because they move with very high acceleration caused by the planes. In **Figure 9**, we preferred to illustrate the nonlinear case of random walk instead of the linear, because the former allows the comparison between gravitation and the movement with acceleration. Indeed, nonlinear random walk stands for a movement equipped with an acceleration which gives the effect of gravitation, though in absence of attraction to cosmic bodies' matter. Therefore, black holes might appear when starting from nonlinear cosmic random walks. Because such acceleration leading to black holes' formation was stronger during the first phases of cosmic expansion, it is feasible to hypothesize that these puzzling cosmic bodies occurred already in the first phases of Universe's development. In touch with this theoretical claim, a newly discovered black hole sits 13.1 billion light years away from us. This means this black hole formed just 690 million years after the Big Bang, 60 million years earlier than the previously oldest-known quasar (Venemans et al., 2017; Bañados et al., 2018). Our approach might also explain what led to the formation of such Universe's most ancient supermassive black holes. Indeed, recent reaserch suggest, in touch with our framework, that those supermassive black holes could have been formed in huge clumps of dark matter that serve as "gravitational glue" for galaxies (Hosokawa et al., 2006; Wise et al., 2019). In this account, the dark matter creates most of the gravity, and then the gas falls into that gravitational potential, where it can form stars or massive black holes.

There are, actually, many ways to generalize the notion of genus to higher dimensions, e.g., Heegaard genus in algebraic topology, arithmetic and geometric genus in algebraic geometry (Almgren and Thurston, 1977). Feldman et al. (1996) tackle the issue of the topological properties of infinite genus Riemann surfaces. They introduce a class of infinite genus Riemann surfaces, specified by means of a number of geometric axioms, to which the classical theory of compact Riemann surfaces up to and including the Torelli Theorem extends. The axioms are flexible enough to encompass many interesting examples, such as the heat curve and a connection to the periodic Kadomcev-Petviashvilli equation. Apart from the mentioned accounts, our results suggest the feasibility of another intriguing operational approach, which allows us to generalize the notion of genus to higher dimensions through another powerful weapon: the Betti number. The 4D Universe might stand for a manifold equipped with a Betti number corresponding to the number of black holes. Betti numbers are topological objects proved to be invariants by Poincaré, and used to extend the polyhedral formula to higher dimensional spaces. Informally, the *k*th Betti number refers to the number of path-connected edges (Kaczynski et al., 2004) embedded in surface holes. For a black hole with *n* vortex cycles and *k* edges attached between each of the cycles,

the Betti number = $n + k$. Ii is noteworthy that Betti numbers play an important role in recent studies of black holes (Manschot et al., 2012).

Our framework might also help to elucidate a puzzling theory: the holographic principle. First proposed by 't Hooft and Susskind, the paradigm is inspired by Bekenstein's and Hawking's account of black hole thermodynamics: the maximal entropy in any region scales with the radius squared, and not cubed. This means that the informational content of objects fallen into a black hole is entirely encompassed in surface fluctuations of the event horizon. The entropy inside the black hole is proportional to the area of the event horizon: in particular, if a black hole's horizon encompasses a number A of Planck areas, its entropy is A/4 units, so that every bit stands for four Planck areas. We ask whether it exists an alternative scenario to the puzzling tenet of the holographic principle, i.e., that the information encompassed in a given volume is endowed in its lower-dimensional surface. Indeed, in the case of a black hole, we might hypothesize that the information is fully located on the 2D surface, while there is no information at all inside the black hole's 3D volume. When an object falls inside a black hole, its information could not cross the horizon reaching the 3D volume inside, rather could be fully retained on the 2D horizon. This means that the proposition "the maximum content of information in cosmic region depends on its area" might not hold true, because, if our hypothesis is confirmed, a black hole's volume might not contain information. This is in touch of our account of empty cells located inside the octahedron produced by nonlinear random walks.

In touch with the experimental data achieved from the Cosmic Background Radiation, our account points towards our Universe as strongly isotropic and homogeneous at cosmic macroscales. According to the current paradigm, inflationary expansion explains why the primeval 10^{90} causally-disconnected quantum "seeds" led to the currently-detected homogeneity and isotropy (Veneziano 21998). Still, inflation would have amplified minute quantum fluctuations (pre-inflation) into slight density ripples of over- and under-density (post-inflation). Is it feasible to correlate our mathematical Pascal's triangles approach to cosmic expansion with the detected isotropy and homogeneity? Here the concept of hyperuniformity comes into play, i.e., the anomalous suppression of density fluctuations on large length scales occurring in amorphous cellular structures of ordered and disordered materials (Klatt et al., 2019). The evolution of a given set of initial points takes place when, through Lloyd iterations, each point is replaced by the centre mass of its Voronoi cell. This corresponds to a gradient descent algorithm which allows a progressive, general convergence to a random minimum in the potential energy surface. Klatt et al. (2019) report that systems equipped with different initial configurations (such as, e.g., either hyperfluctuating, or anisotropic, or relatively homogeneous pointsets), converge towards the same high degree of uniformity after a relatively small number of Lloyd iterations (about 10^5). This means that, in the systems' final states, independent of the initial conditions, the cell volumes become uniform and the dimensionless total energy converges towards values comparable to the optimal lattice's deep local energy minima. Therefore, we are allowed to describe the cosmic evolution suddenly after the Big Bang in terms of Lloyd iterations, where the initial quantum seeds stand for initial point sets, progressively converted to point sets with a centroidal Voronoi diagram. In other words, the tiny perturbations in the primordial universe which seed the later formation of cosmic macro-structures might stand for the starting points of the subsequent processes described by Klatt et al. (2019) in terms of Voronoi cells, and by us in terms of Pascal's triangle models. This would permit us observers to achieve, starting from countless different possible conformations of the primeval Universe, the currenlty detected isotropic and homogeneous Cosmic Background Radiation. Indeed, after just 10^5 iterations, every possible initial system must converge towards an hyperuniform state, where the observers perceive energy as very low and the degree of uniformity as very high.

REFERENCES

1) Ahmad MZ, Peters JF. 2019. Proximity induced by order relations. arXiv, 1903.05532v2, 1-22.
2) Askar'yan G, Yurkin A. 1989. New developments in optoacoustics. Sov. Phys. Usp. 32 (4):349 – 356.
3) Almgren FJ Jr, Thurston WP. 1977. Examples of Unknotted Curves Which Bound Only Surfaces of High Genus Within Their Convex Hulls. Annals of Mathematics. Second Series, Vol. 105(3):527-538. DOI: 10.2307/1970922
4) Bañados E, Venemans BP, Mazzucchelli C, Farina EP, Walter F, et al. 2018. An 800-million-solar-mass black hole in a significantly neutral Universe at a redshift of 7.5. Nature, 553, 473–476.
5) Brothers HJ. 2012. Finding e in Pascal's triangle. Mathematics Magazine, 85: 51. doi:10.4169/math.mag.85.1.51
6) Edwards AWF. 2013. The arithmetical triangle. In Wilson, Robin; Watkins, John J., Combinatorics: Ancient and Modern, Oxford University Press, pp. 166–180.
7) Einstein A. 1905. ZurElektrodynamikbewegterKörper. Annalen der Physik (Berlin) (in German), Hoboken, NJ (published 10 March 2006), 322 (10), pp. 891–921, Bibcode:1905AnP...322..891E

8) Fedotov S, Korabel N. 2015. Nonlinear and non-Markovian random walk: self-organized anomaly. arXiv:1505.02625v1.
9) Feldman J, Knörrer H, Trubowitz E. 1996. Infinite Genus Riemann Surfaces, Toronto 1995.in Canadian Mathematical Society/ Société mathématique du Canada 1945-1995. Volume/Tome 3. Edited by James B. Carrell and Ram Murty, Canadian Mathematical Society, Ottawa (1996) 91-112.
10) Hore PJ. 1983. Solvent suppression in Fourier transform nuclear magnetic resonance. Journal of Magnetic Resonance, 55 (2): 283–300. doi:10.1016/0022-2364(83)90240-8.
11) Hosokawa T, Yorke HW, Inayoshi K, Omukai K., Yoshida N. 2013. Formation of primordial supermassive stars by rapid mass accretion. Astrophys J 778, 178.
12) Kaczynski, T., Mischaikov, K., Mrozek, M. 2004. Computational Homology. Springer-Verlag, NY, ISBN 0-387-40853-3.
13) Klatt MA, Lovrić J, Chen D, Kapfer SC, Schaller FM, et al. 2019. Universal hidden order in amorphous cellular geometries. Nature Communications, 10:811.
14) Klein F. *1956.* About so-called non-Euclidean geometry. About the geometry bases. Collection of classical works on Lobachevsky's geometry and development of its ideas. Moscow: Gosizdat.
15) Kolmogorov A, Zhurbenko I, Prokhorov A. 1995. Introduction to the theory of probability. Moscow: Nauka.
16) Manschot, J., Pioline, B., Sen, A. 2012. From black holes to quivers. High Energy Physics doi:10.1007/JHEP11(2012)023.
17) Peters JF. 2018. Proximal vortex cycles and vortex nerve structures. Non-concentric, nesting, possibly overlapping homology cell complexes. Journal of Mathematical Sciences and Modelling 1, no. 2, 80-85. ISSN 2636-8692.
18) Peters JF. 2019. Computational Geometry, Topology and Physics. Shape Complexes, Optical Vortex Nerves and Proximities in Digital Images. Springer Int. Pub., 2019, in press.
19) Sarkar J, Maiti SI. 2017. Symmetric Random Walks on Regular Tetrahedra, Octahedra, and Hexahedra. Calcutta Statistical Association Bulletin (2017) 69(1) 110–128.
20) Sommerfeld A. 1973. Cognition Ways in Physics. Collection of papers, p. 157. Editor: Smorodinsky J. Moscow: Nauka. (Klein, Riemann und die mathematische Physik. Naturwiss (1919), 7.
21) Venemans BP, Walter F, Decarli R, Bañados E, Carilli C, et al. 2017. Copious Amounts of Dust and Gas in a z = 7.5 Quasar Host Galaxy. The Astrophysical Journal Letters, 851 (1).
22) Veneziano G. 1998. A Simple/Short Introduction to Pre-Big-Bang Physics/Cosmology. arXiv:hep-th/9802057v2
23) Weyl H. 1955. The Concept of a Riemann Surface, trans. By G.R. MacLane, Dover Pub. Inc., NY, 191 pp.
24) Wise JH, Regan JA, O'Shea BW, Norman ML, Downes TP, Xu H. 2019. Formation of massive black holes in rapidly growing pre-galactic gas clouds. Nature, 566, 85–88.
25) Yurkin A. 1995. System of rays in lasers and a new feasibility of light coherence control. (1995) Optics Communications, v.114, p. 393.
26) Yurkin A. 2013. New binomial and new view on light theory. About one new universal descriptive geometric model. (2013) Lambert Academic Publishing, ISBN 978-3-659-38404-2.
27) Yurkin A. 2016. On descriptive geometrical interpretation of the principle of Pauli, elements of the table of Mendeleyev and the Newtonian laminar current of liquid. (2016) Progress in physics, 12: 149-169.
28) Yurkin A. 2018. And where are fluctuations in quantum-mechanical wave function? Advances in Theoretical & Computational Physics, v. 1. Issue 1.1 -7.
29) Yurkin A, Tozzi A, Peters JF, Marijuán P. 2017. Quantifying Energetic Dynamics in Physical and Biological Systems Through a Simple Geometric Tool and Geodetic Curves. Progress in Biophysics and Molecular Biology 131: 153-161.
30) Yurkin A, Peters JF, Tozzi A. 2018. A novel belt model of the atom, compatible with quantum dynamics. Journal of Scientific and Engineering Research 5(7):413-419. www.jsaer.com.
31) A Yurkin. 2019. Computing Stiks against Random Walk (2019) Advances in Theoretical & Computational Physics, v. 2. Issue 1.1 -6.